Acknowledgment. The support of the National Institutes of Health (Grant GM 25172) is gratefully acknowledged. We also acknowledge helpful discussions concerning the ESR spectra with Dr. David Bocian.

Registry No. [[(*p*-Et_2N)TPP]Fe]$_2O$, 89177-90-2; [(*p*-Et_2N)TPP]FeCl, 85529-39-1; [$(CN)_4$TPP]FeCl, 96293-36-6; [[$(CN)_4$TPP]Fe]$_2O$, 69968-24-7; [[$(CN)_4$TPP]Fe]$_2O^-$, 96293-37-7; [[$(CN)_4$TPP]Fe]$_2O^{2-}$, 96293-38-8; [[$(CN)_4$TPP]Fe]$_2O^{3-}$, 96293-39-9; [[$(CN)_4$TPP]Fe]$_2O^{4-}$, 96293-40-2; [(*p*-Et_2N)TPP]FeCl$^+$, 96293-41-3; [(*p*-Et_2N)TPP]FeCl^{2+}, 96293-42-4; [(*p*-Et_2N)TPP]FeCl^{4+}, 96293-43-5; [(*p*-Et_2N)TPP]Fe, 96293-44-6; [(*p*-Et_2N)TPP]Fe$^-$, 96293-45-7; (TPP)Fe$^-$, 54547-68-1; [$(CN)_4$TPP]Fe$^-$, 96293-46-8; [$(CN)_4$TPP]Fe, 96293-47-9; [$(CN)_4$TPP]Fe^{2-}, 96293-48-0; TBAP, 1923-70-2; (TBA)PF_6, 3109-63-5.

Contribution from the Department of Chemistry, Massachusetts Institute of Technology, Cambridge, Massachusetts 02139

Electronic and Vibrational Spectroscopic Analysis of the (μ-Oxo)bis(μ-carboxylato)diiron(III) Core: A Study of $[Fe_2O(O_2CCH_3)_2(TACN)_2]^{2+}$

ALAN SPOOL, IAN D. WILLIAMS, and STEPHEN J. LIPPARD*

Received October 26, 1984

Comparison of the electronic and vibrational spectroscopic properties of the two hemerythrin model compounds $[Fe_2O(O_2CCH_3)_2(TACN)_2]I_2{\cdot}0.5CH_3CN$ (**1**) and $[Fe_2O(O_2CCH_3)_2(HB(pz)_3)_2]$ (**2**) (TACN = 1,4,7-triazacyclononane and $HB(pz)_3^-$ = hydrotris(1-pyrazolyl)borate anion) has enabled identification of features characteristic of the (μ-oxo)bis(μ-carboxylato)diiron(III) core. Raman spectral studies of **1** show ν_s(Fe–O–Fe) to occur at 540 cm^{-1}, shifting to 523 cm^{-1} in [^{18}O]**1**. From difference Fourier transform infrared spectral measurements, the corresponding ν_{as}(Fe–O–Fe) bands were located at 749 cm^{-1} and, for [^{18}O]**1**, 716 cm^{-1}. Electronic spectral transitions between 300 and 500 nm in both **1** and **2** are shown to be diagnostic of the $[Fe_2O(O_2CCH_3)_2]^{2+}$ core. In protic solvents, the optical bands in **1** shift in both frequency and intensity, a result attributed to hydrogen bonding to the oxo bridge. Also reported for **1** are studies of its aqueous solution instability, excitation profiles in the Raman spectrum measured from 454 to 577 nm, and the results of an X-ray crystal structure analysis. The relevance of these studies to the binuclear iron center in hemerythrin is discussed.

Introduction

Recently we prepared and characterized models[1] for the active site of hemerythrin (Hr),[2] the marine invertebrate oxygen transport protein. Our initial objective was to study the (μ-oxo)bis(μ-carboxylato)diiron(III) core, a species identified in the crystal structures of azidomethemerythrin and azidometmyohemerythrin and a likely structure in the bimetallic core of some ribonucleotide reductases (RR).[1,4] An independent report[5] describes the synthesis of a complex containing this same diiron core, but with a capping ligand (1,4,7-triazacyclononane (TACN)) different from the one employed by us, hydrotris(1-pyrazolyl)borate anion ($HB(pz)_3^-$). The resulting cationic complex $[Fe_2O(O_2CCH_3)_2(TACN)_2]^{2+}$ is of similar composition and structure.

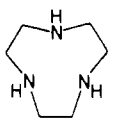

TACN
[9]-ane-N_3

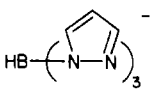

$HB(pz)_3^-$

Among the many physical properties studied for Hr, RR, and related proteins, electronic and vibrational spectra have been most useful in characterizing and identifying the $[Fe_2O(O_2CR)_2]^{2+}$ core. We were therefore interested to learn the degree to which changing the nonbridging ligand from $HB(pz)_3^-$ to TACN would influence these properties in the model compounds. Such a comparison also facilitates assignment of the protein electronic and vibrational spectra. We have therefore undertaken a detailed study of the electronic, resonance Raman and infrared spectra of the (μ-oxo)bis(μ-carboxylato)bis([9]-ane-N_3)diiron(III) cation, the results of which are reported here.

Experimental Section

Materials and Methods. [^{18}O]H_2O (99%) was purchased from Stohler Isotope Chemicals, Waltham, MA. All other reagents, with the exception of the acetonitrile used in the isotope-exchange experiment, were obtained from commerical sources and used without further purification.

Preparation of $[Fe_2O(O_2CCH_3)_2(TACN)_2]I_2{\cdot}0.5CH_3CN$ (1). The complex was prepared as described in the literature,[5] except that in our hands the product of the precipitation with NaI was an orange-brown powder. This material was dissolved in a minimum amount of hot CH_3CN, and the resulting solution was cooled slowly to room temperature. The solution was then allowed to stand at 4 °C for 24 h while brown crystals formed. Since the unit cell and space group of these stable crystals differed from those originally reported,[5] we decided to undertake a complete X-ray structural investigation. The results of this study revealed the presence of acetonitrile in the lattice, which was confirmed by chemical analysis and proton NMR spectroscopy. Anal. Calcd for $Fe_2I_2O_5N_{6.5}C_{17}H_{37.5}$: C, 26.23; H, 4.86; N, 11.69; I, 32.6. Found: C, 25.94; H, 4.95; N, 11.27; I, 34.2. NMR analysis: From the integrated intensity of the proton resonances of a weighed sample of the compound dissolved in CH_3CN-d_3 with $CHCl_3$ as an internal standard, the ratio of acetonitrile molecules to diiron units in compound **1** was measured to be 0.6.

Preparation of [^{18}O][$Fe_2O(O_2CCH_3)_2(TACN)_2$]$I_2$. ^{18}O enrichment of the bridging position in **1** for vibrational spectroscopic studies was accomplished as follows.[1b] Acetonitrile, distilled from calcium hydride under nitrogen, was transferred under nitrogen to a flask containing 50 mg of **1**. After the solid was completely dissolved, 100 μL of [^{18}O]H_2O was syringed into the vessel and the mixture was allowed to stir overnight. The solvent was then removed in vacuo, and the resulting solid was used without further purification. The infrared spectrum of **1** treated in this way with [^{16}O]H_2O was identical with that of the untreated material.

Physical Measurements. ^{1}H NMR spectra were recorded with a Bruker WM 250 spectrometer. Electronic absorption spectra in the range 250–800 nm were recorded with a Cary Model 118C spectropho-

(1) (a) Armstrong, W. H.; Lippard, S. J. *J. Am. Chem. Soc.* **1983**, *105*, 4837–4838. (b) Armstrong, W. H.; Spool, A.; Papaefthymiou, G. C.; Frankel, R. B.; Lippard, S. J. *J. Am. Chem. Soc.* **1984**, *106*, 3653–3667.
(2) (a) Klotz, I. M.; Klippenstein, G. L.; Hendrickson, W. A. *Science (Washington, D.C.)* **1976**, *192*, 335–344. (b) Kurtz, D. M., Jr.; Shriver, D.; Klotz, I. M. *Coord. Chem. Rev.* **1977**, *24*, 145–178. (c) Stenkamp, R. E.; Jensen, L. H. *Adv. Inorg. Biochem.* **1979**, *1*, 219–233. (d) Sanders-Loehr, J.; Loehr, T. M. *Adv. Inorg. Biochem.* **1979**, *1*, 235–252. (e) Wilkins, R. G.; Harrington, P. C. *Adv. Inorg. Biochem.* **1983**, *5*, 51–85. (f) Klotz, I. M.; Kurtz, D. M., Jr. *Acc. Chem. Res.* **1984**, 16–22.
(3) (a) Hendrickson, W. A. In "Invertebrate Oxygen-Binding Proteins: Structure, Active Site, and Function"; Lamy, J., Lamy, J., Eds.; Marcel Dekker: New York, 1981; pp 503–515. (b) Hendrickson, W. A.; Sheriff, S.; Smith, J. L., private communication. (c) Stenkamp, R. E.; Sieker, L. C.; Jensen, L. H.; Sanders-Loehr, J. *Nature (London)* **1981**, *291*, 263–264. (d) Stenkamp, R. E.; Sieker, L. C.; Jensen, L. H. *J. Am. Chem. Soc.* **1984**, *106*, 618–622. (e) Stenkamp, R. E.; Sieker, L. C.; Jensen, L. H. *Acta Crystallogr., Sect. B: Struct. Crystallogr. Cryst. Chem.* **1982**, *B38*, 784–792. (f) Stenkamp, R. E.; Sieker, L. C.; Jensen, L. H. *J. Inorg. Biochem.* **1983**, *19*, 247–253.
(4) (a) Sjöberg, B.-M.; Gräslund, A. *Adv. Inorg. Biochem.* **1983**, *5*, 87–110. (b) Reichard, P.; Ehrenberg, A. *Science (Washington, D.C.)* **1983**, *221*, 514–519. (c) Lammers, M.; Follmann, H. *Struct. Bonding (Berlin)* **1983**, *54*, 27–91.
(5) Wieghardt, K.; Pohl, K.; Gebert, W. *Angew. Chem., Int. Ed. Engl.* **1983**, *22*, 727.

0020-1669/85/1324-2156$01.50/0

Table I. Experimental Details of the X-ray Diffraction Study of $[Fe_2O(O_2CCH_3)_2(TACN)_2]I_2 \cdot 0.5CH_3CN$

(A) Crystal Parameters[a,b]

a = 15.968 (2) Å	space group: $I4_1cd$
c = 24.821 (2) Å	Z = 8
V = 6328.8 Å^3	ρ(calcd) = 1.634 g cm^{-3}
	mol wt = 778.5

(B) Measurement and Treatment of Intensity Data[c]

instrument: Enraf Nonius CAD-4F κ-geometry diffractometer
radiation: Mo Kα (λ = 0.71073 Å), graphite monochromatized
standards: (3,2,$\bar{11}$), (5,5,6), ($\bar{8}$,6,$\bar{4}$); monitored every 3600 s, varied randomly with no overall decay in the average of the three standards
no. of reflcns collcd exclusive of syst absences: 2968 [3° ≤ 2θ ≤ 60°] (+h,+k,+l)
abs cor
cryst size: 0.3 × 0.3 × 0.3 mm
linear abs coeff: 27.8 cm^{-1}
transmission factors: 0.43–0.53
cryst faces: {112}; {$\bar{1}$12}; {$\bar{1}\bar{1}$2}; {1$\bar{1}$2}
R_{av}[e]: 0.025
no. of reflcns after averaging: 2353

(C) Final Model in Least-Squares Refinement

final R values[e]	R_1 = 0.0385, R_2 = 0.0493
no. of observns	1652 [$F_o > 4\sigma(F_o)$]
no. of variable params	158

[a] From a least-squares fit to the setting angles of 25 reflections with 2$\theta \geq 20°$. [b] Unit cell parameters and data collection at 24 ± 1 °C. [c] See ref 8 for further details. [d] Absorption correction was applied with the Wehe–Busing–Levy ORABS program. [e] $R_1 = \sum||F_o| - |F_c||/\sum|F_o|$; $R_2 = [\sum w(|F_o|^2 - |F_c|^2)/\sum w|F_o^2|]^{1/2}$.

tometer and above 800 nm with a Perkin-Elmer Model 330 spectrophotometer. Infrared spectra were recorded with a Perkin-Elmer Model 283B spectrometer, and FTIR data were obtained on a Nicolet 7199 Fourier transform spectrometer. Raman spectra were recorded as described previously,[1b] with the following differences. Data were stored in a Tetronix computer interfaced to the Raman spectrometer. To improve the signal-to-noise ratio, scans were computer-averaged two times for medium to strong peaks and three times for weak peaks. All spectra were obtained by using 40–55 mW of power incident at the sample.

A sealed 5-mm NMR tube containing a filtered, nearly saturated solution of **1** in CH_3CN was prepared and used for all solution Raman spectral work. The excitation profile was determined as previously described[1b] by using the 917-cm^{-1} peak of the solvent as a standard. A sealed 5-mm NMR tube of [^{18}O]**1** in CH_3CN was prepared by using CH_3CN freshly distilled from calcium hydride under nitrogen.

Collection and Reduction of X-ray Data for $[Fe_2O(OCCH_3)_2(TACN)]I_2 \cdot 0.5CH_3CN$ (1). Crystals of **1** were grown from an acetonitrile solution at 4 °C. The crystal used for data collection was a tetragonal bipyramid, which appeared red under transmitted polarized light. There was no apparent deterioration of the sample in air so the crystal used for data collection was mounted on the end of a glass fiber. The crystal quality was found to be acceptable on the basis of ω scans of several low-angle reflections ($\overline{\Delta\omega_{1/2}}$ = 0.2°). Compound **1** crystallizes in the tetragonal system, Laue symmetry 4/mmm, with systematic absences consistent only with space group $I4_1cd$ (No. 110).[6] Crystal parameters and additional details of the data collection and reduction are given in Table I and ref 7.

Structure Solution and Refinement. The structure was solved by standard Patterson and difference Fourier methods and refined by using anisotropic thermal parameters for all non-hydrogen atoms. Neutral-atom scattering factors and anomalous dispersion corrections for non-hydrogen atoms were taken from ref 8 and hydrogen atom scattering factors from ref 9. All hydrogen atoms were placed at calculated positions with d(C–H) = 0.95 Å. The methyl groups were treated as rigid bodies with three rotational variables each. The methylene hydrogens were constrained to "ride" on the carbon atoms to which they were attached.[10] Hydrogen atoms were given a fixed isotropic thermal parameter (U = 0.1 Å^2).

Three peaks of significant electron density (between 1.0 and 2.0 e Å^{-3}), located near a 2-fold symmetry axis but not proximal to either the dimer cation or its iodide counterions, were revealed at the latter stages of refinement. These were identified, chemically and spectroscopically (vide supra) as well as crystallographically, to be a molecule of acetonitrile, disordered about the 2-fold axis. For refinement this molecule was constrained to have idealized geometry (C–N = 1.1 Å; C–C = 1.5 Å) and was positioned on the 2-fold axis. All three atoms were assigned anisotropic thermal parameters to simulate the disorder through librational motion normal to the symmetry axis. The atoms were also given half-occupancy in accord with the chemical and NMR data.

The function minimized during refinement was $\sum w(|F_o| - |F_c|)^2$, where $w = 1.8020/[\sigma^2(F_o) + 0.0005(F_o)^2]$. Toward the end of the refinement a test was made to check that the choice of polarity was correct. The largest ratio of parameter shift to estimated standard deviation in the final cycle of refinement was <0.1 except for parameters of the acetonitrile solvent molecule. The largest peak of residual electron density was 1.2 e Å^{-3}, associated with the iodide ions. All other residual peaks were ≤±0.5 e Å^{-3}. Final positional parameters are presented in Table II and a list of interatomic distances and angles is given in Table III. Table S1 contains a listing of structure factors, and Table S2 has the final thermal parameters for non-hydrogen atoms.[11]

Table II. Atomic Positional Parameters for $[Fe_2O(O_2CCH_3)_2(TACN)_2]I_2 \cdot 0.5CH_3CN$[a]

ATOM	X	Y	Z
I1	0.28329(4)	0.12686(4)	0.0000
Fe1	0.55146(6)	0.08095(6)	0.08251(5)
O1	0.4553(4)	0.1105(4)	0.1334(3)
O2	0.3837(4)	-0.0083(4)	0.1358(2)
O3	0.5000	0.0000	0.0459(3)
N1	0.6192(5)	0.1899(4)	0.1154(4)
H1N	0.6128(5)	0.1956(4)	0.1533(4)
N2	0.6593(5)	0.0872(4)	0.0302(3)
H2N	0.6899(5)	0.0366(4)	0.0261(3)
N3	0.5129(5)	0.1798(4)	0.0276(3)
H3N	0.4567(5)	0.1741(4)	0.0157(3)
C1	0.3912(5)	0.0682(5)	0.1441(3)
C2	0.3196(7)	0.1139(7)	0.1702(6)
H2A	0.2782(7)	0.0998(7)	0.1443(6)
H2B	0.3234(7)	0.1731(7)	0.1732(6)
H2C	0.3047(7)	0.0907(7)	0.2041(6)
C12	0.7073(7)	0.1809(11)	0.1026(6)
H12A	0.7301(7)	0.1457(11)	0.1297(6)
H12B	0.7349(7)	0.2336(11)	0.1034(6)
C21	0.7233(8)	0.1426(9)	0.0527(10)
H21A	0.7341(8)	0.1865(9)	0.0278(10)
H21B	0.7720(8)	0.1091(9)	0.0567(10)
C13	0.5872(11)	0.2698(6)	0.0926(7)
H13A	0.6310(11)	0.2988(6)	0.0745(7)
H13B	0.5678(11)	0.3027(6)	0.1219(7)
C31	0.5163(9)	0.2607(5)	0.0570(5)
H31A	0.4656(9)	0.2664(5)	0.0767(5)
H31B	0.5201(9)	0.3042(5)	0.0310(5)
C23	0.6302(9)	0.1110(9)	-0.0225(5)
H23A	0.6039(9)	0.0624(9)	-0.0366(5)
H23B	0.6751(9)	0.1270(9)	-0.0455(5)
C32	0.5668(9)	0.1771(10)	-0.0212(5)
H32A	0.5962(9)	0.2284(10)	-0.0250(5)
H32B	0.5299(9)	0.1699(10)	-0.0509(5)
N1S	0.0000	0.0000	0.1114(16)
C1S	0.0000	0.0000	0.0680(14)
C2S	0.0000	0.0000	0.0085(14)

[a] Numbers in parentheses are errors in the last significant digit(s). [b] Atoms are labeled as shown in Figure 1.

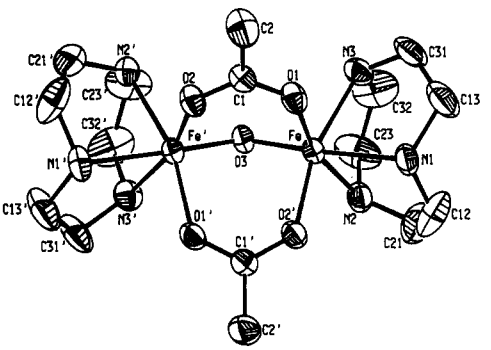

Figure 1. Structure of **1** showing the 40% probability thermal ellipsoids.

(6) "International Tables for X-ray Crystallography", 3rd ed.; Kynoch Press: Birmingham, England, 1973; Vol. I, p 200.
(7) Silverman, L. D.; Dewan, J. C.; Giandomenico, C. M.; Lippard, S. J. *Inorg. Chem.* **1980**, *19*, 3379–3383.
(8) "International Tables for X-ray Crystallography"; Kynoch Press: Birmingham, England, 1974; Vol. IV, pp 99, 149.
(9) Stewart, R. F.; Davidson, E. R.; Simpson, W. T. *J. Chem. Phys.* **1965**, *42*, 3175–3187.
(10) SHELX-76: Sheldrick, G. M. In "Computing in Crystallography"; Schenck, H., Olthof-Hazenkamp, R., van Koningsveld, H., Bassi, G. C., Eds.; Delft University Press: Delft, The Netherlands, 1978; pp 34–42.

Table III. Bond Lengths (Å) and Angles (deg) for $[Fe_2O(O_2CCH_3)_2(TACN)_2]I_2 \cdot 0.5CH_3CN$[a]

Coordination Sphere		
	Å or deg	
Fe1···Fe1'	3.063(2)	[3.064(5)]
Fe1-O1	2.043(6)	[2.04;2.00]
Fe1-O2'	2.041(6)	[2.03;2.05]
Fe1-O3	1.781(4)	[1.77;1.80]
Fe1-N1	2.205(7)	[2.20;2.21]
Fe1-N2	2.158(7)	[2.16;2.17]
Fe1-N3	2.173(6)	[2.16;2.17]
Fe1-O3-Fe1'	118.7(4)	[118.3(5)]
O1-Fe1-N2	163.8(2)	
O2'-Fe1-N3	164.3(3)	
O3-Fe1-N1	171.1(3)	
O1-Fe1-O2'	96.4(3)	
O1-Fe1-O3	97.8(2)	
O2'-Fe1-O3	98.7(2)	
O1-Fe1-N1	87.5(3)	
O1-Fe1-N3	90.4(3)	
O2'-Fe1-N1	87.7(3)	
O2'-Fe1-N2	90.7(3)	
O3-Fe1-N2	95.5(3)	
O3-Fe1-N3	94.4(3)	
N1-Fe1-N2	78.2(3)	
N1-Fe-N3	78.4(3)	
N2-Fe1-N3	79.4(3	
Ligand Geometries		
Acetate Group		
C1-O1	1.255(10)	[1.26,1.27]
C1-O2	1.245(10)	[1.23,1.26]
C1-C2	1.503(13)	[1.49,1.51]
$O_1 \cdots O_2$	2.217(8)	
O1-C1-O2 124.9(8)	Fe1-O1-C1	128.3(5)
O1-C1-C2 116.8(8)	Fe1-O2'-C1'	128.2(5)
O2-C1-C2 118.3(8)		
1,4,7-triazacyclononane		
N1-C12	1.450(15)	
N1-C13	1.488(13)	
N2-C21	1.461(15)	
N2-C23	1.442(15)	
N3-C31	1.485(12)	
N3-C32	1.487(14)	
C12-C21	1.405(23)	
C13-C31	1.443(18)	
C23-C32	1.462(18)	
Fe1-N1-C12	108.5(8)	
Fe1-N1-C13	111.6(7)	
C12-N1-C13	109.5(1.1)	
Fe1-N2-C21	110.9(8)	
Fe1-N2-C23	107.5(7)	
C21-N2-C23	114.4(1.2)	
Fe1-N3-C31	108.3(6)	
Fe1-N3-C32	109.0(6)	
C31-N3-C32	113.8(1.0)	
N1-C12-C21	114.3(1.0)	
N1-C13-C31	114.6(9)	
N2-C21-C12	118.2(1.1)	
N2-C23-C32	113.1(1.0)	
N3-C31-C13	114.6(9)	
N3-C32-C23	116.1(1.0)	

[a] Atoms are labeled as shown in Figure 1. Numbers in brackets are values from the structure determination of $[Fe_2O(O_2CCH_3)_2(TACN)_2]I_2 \cdot 0.5NaI \cdot 3H_2O$.[5]

Results and Discussion

Description of the X-ray Structure of $[Fe_2O(O_2CCH_3)_2(TACN)_2]I_2 \cdot 0.5CH_3CN$ (1). The cation geometry (Figure 1) is essentially identical with that communicated previously for $[Fe_2O(O_2CCH_3)_2(TACN)_2]I_2 \cdot 0.5NaI \cdot 3H_2O$.[5] In **1**, however, the halves of the cation are related by a crystallographic 2-fold symmetry axis passing through the bridging oxygen atom O(3). Bond lengths and angles for the two structure determinations are in excellent agreement, within the reported error limits, where available for comparison with the earlier published results (Table III).

The geometry of the $[Fe_2O(O_2CCH_3)_2]^{2+}$ core in **1** exhibits only minor changes from that of the $[Fe_2O(O_2CCH_3)_2(HB(pz)_3)_2]$ analogue, **2**.[1] In particular, the Fe···Fe internuclear separation is slightly smaller (3.063 (2) Å vs. 3.1457 (6) Å), a consequence of the less obtuse Fe–O–Fe angle (118.7 (4)° vs. 123.6 (1)°). The source of these differences is uncertain. As in the $HB(pz)_3^-$ derivative, the Fe–N bonds trans to the bridging oxygen atom are significantly lengthened relative to the others, a result previously ascribed to the greater structural trans effect of the μ-oxo ligand.[1]

The steric requirements of the TACN and $HB(pz)_3^-$ ligands are not identical, although roughly similar as seen by comparison of the N–Fe–N angles. A greater deviation from the idealized orthogonal geometry is found for TACN, the N–Fe–N angles ranging between 78.2 (3) and 79.4 (3)°, whereas in **2** the N–Fe–N angles fall between 81.7 (1) and 84.9 (1)°.

The geometry of the TACN ligand is otherwise unremarkable. Comparatively short C–C bond lengths between the methylene groups of the ligand (average 1.43 (2) Å) may be attributed to the effects of libration, since large anisotropic thermal parameters are associated with these carbon atoms. The hydrogen atoms on the TACN nitrogen atoms were not directly located in the crystal structure analysis. The computer-generated positions for these atoms gave the closest contacts to the iodide counterions, ranging from 2.72 to 2.89 Å and suggesting a partial degree of hydrogen-bond character. This observation has been noted previously in amine/iodide salts[12] and may account for the propensity of cationic crystals of TACN complexes to crystallize nicely with iodide counterions.

Electronic Spectra. A list of peaks from the electronic spectra of **1** in three different solvents is given in Table IV along with comparable results for other oxo-bridged diiron(III) complexes, hemerythrin derivatives, and ribonucleotide reductase.[13-17] Of particular interest is the similarity between the spectra of **1** in CH_3CN and CH_3OH and that of $[Fe_2O(O_2CCH_3)_2(HB(pz)_3)_2]$ (**2**).[1] The peaks between 300 and 400 nm, usually a strong absorption at higher energy with a lower energy shoulder, seem to be characteristic of the oxo bridge and appear in all of the spectra listed in Table IV. In other oxo-bridged complexes, these bands are often poorly resolved shoulders on more intense higher energy bands.[18]

As in the spectra of hemerythrin[13] and **2**,[1] only the two lowest energy d–d bands can be observed in the spectra of **1**, since the others are obscured by other more intense transitions. In CH_3OH these absorptions occur at 1020 and 743 nm. Their positions compared to those in the spectrum of **2** suggest that TACN is a slightly weaker field ligand than $HB(pz)_3^-$. In organic solvents, the extinction coefficients of these bands are similar to those of comparable bands in the spectra of **2**, hemerythrin, and ribonucleotide reductase. In the spectra of simple oxo-bridged complexes these bands are also greatly enhanced by comparison to mononuclear, high-spin, octahedrally coordinated iron(III) complexes but are still less intense than the bands in the spectra of

(11) Supplementary material.

(12) Corfield, P. W. R.; Baltusis, L. M.; Lippard, S. J. *Inorg. Chem.* **1981**, *20*, 922–929.
(13) (a) Sanders-Loehr, J.; Loehr, T. M.; Mauk, A. G.; Gray, H. B. *J. Am. Chem. Soc.* **1980**, *102*, 6992–6996. (b) Dunn, J. B. R.; Addison, A. W.; Bruce, R. E.; Sanders-Loehr, J.; Loehr, T. M. *Biochemistry* **1977**, *8*, 1743–1749. (c) Garbett, K.; Darnall, D. W.; Klotz, I. M.; Williams, R. J. P. *Arch. Biochem. Biophys.* **1969**, *103*, 419–434.
(14) Schugar, H. J.; Rossman, G. R.; Barraclough, C. G.; Gray, H. B. *J. Am. Chem. Soc.* **1972**, *94*, 2683–2690.
(15) Armstrong, W. H.; Lippard, S. J. *J. Am. Chem. Soc.* **1984**, *106*, 4632–4633.
(16) Armstrong, W. H., personal communication.
(17) (a) Petersson, L.; Gräslund, A.; Ehrenberg, A.; Sjöberg, B.-M.; Reichard, P. *J. Biol. Chem.* **1980**, *255*, 6706–6712. (b) Brown, N. C.; Eliasson, R.; Reichard, P.; Thelander, L. *Eur. J. Biochem.* **1969**, *9*, 512–518.
(18) Murray, K. S. *Coord. Chem. Rev.* **1974**, *12*, 1–35.

Table IV. Electronic Spectral Data[a]

$[Fe_2O(O_2CCH_3)_2(TACN)_2]I_2 \cdot 0.5CH_3CN$		$[Fe_2O(O_2CCH_3)_2(HB(pz)_3)_2]$[b]	$[Fe_2O(HB(pz)_3)_2(H_2B(pz)_2)_2]$[c]	$enH_2(Fe_2O(HEDTA)_2]$[d]	hemerythrin derivatives[e]			ribonucleotide reductase[f]	$[Fe_2(OH)(O_2CCH_3)_2(HB(pz)_3)_2]ClO_4$[g]
in CH_3CN	in MeOH	in H_2O				azidomet	oxy	hydroxy		
280 (sh)	275 (sh)		262 (3375)	269 (6400)	235 (>1000)	---------- protein absorption ----------				
			306 (5200)		307 (>1000)					
333 (3682)	335 (3679)	323 (2979)	339 (4635)		343 (>1000)	326 (3375)	330 (3400)	320 (3400)	325 (4700)	
368 (sh)	373 (sh)	374 (sh)	358 (sh)			380 (sh)	360 (sh)	362 (2950)	370 (3600)	375 (5300, br)
420 (sh)	420 (sh)	413 (sh)		382 (5300)	403 (120)					
468 (655)	464 (537)	448 (399)	457 (505)		455 (sh)	446 (1850, br)				
492 (sh)	489 (sh)	491 (sh)	492 (466)		477 (25)			480 (sh)		
508 (sh)	506 (398)						500 (1100, br)		500 (400, br)	
544 (sh)	543 (sh)		528 (sh)		540 (40)					
745 (71)	743 (66)	701 (41)	695 (70)	750 (sh)		680 (95)	750 (100)	597 (80)	600 (150)	700 (sh)
	1020 (3.2)		955 (3.5)		894 (2.6)	1010 (5.1)	990 (5.0)	990 (4.0)	not reported	1115 (0.9)

[a] Absorption maxima are reported in nm with molar extinction coefficients per iron in parentheses. [b] Reference 1. [c] Armstrong, W. H.; Lippard, S. J., unpublished results. [d] Reference 14. [e] Reference 17. [f] References 15, 16.

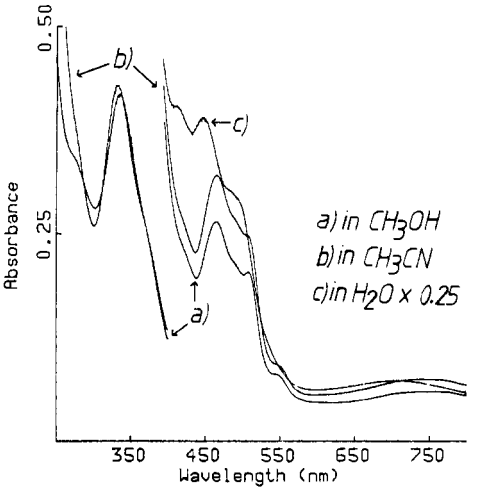

Figure 2. Electronic spectra of **1** in various solvents. Spectra shown are of 2.0 mM **1** in H_2O (×0.25), 0.25 mM **1** in CH_3CN, and 0.25 mM **1** in CH_3OH.

1, **2**, and the proteins. The enhancement of the d–d transitions in the spectra of oxo-bridged compounds in general, and in the spectra of hemerythrin specifically, has been ascribed[13a,14] to lowered symmetry, spin–spin interactions between the metal ions, or both.

The series of bands between 400 and 550 nm with extinction coefficients of 300–600 cm^{-1} M_{Fe}^{-1} appear to be specific for oxo-bridged compounds containing additional bridging carboxylate ligands. In the spectra of protein derivatives having no ligand-to-metal charge-transfer bands in this region, broad, unresolved absorptions occur between 400 and 550 nm.[13,17] In the spectrum of **2**, two well-resolved bands can be seen at 457 and 492 nm, but they do not appear to be simple curves, indicating that there may be more than two transitions contributing to these absorptions. The intensities and positions of the peaks in this part of the spectrum of **1** are similar to those observed in the spectra of **2** and the proteins, but extra shoulders are evident. No fewer than five different bands and shoulders between 400 and 550 nm can clearly be delineated in the spectrum of **1** in methanol (Figure 2).

The similarity in appearance of the spectra of **1** and **2** reveals that no pyrazole-to-metal charge-transfer bands occur in the spectrum of the latter since none of its spectral bands is absent in that of the TACN derivative. Because pyrazole and imidazole complexes have similar electronic structures[19] and, more importantly, since neither hemerythrin nor ribonucleotide reductase has any intense extra bands in its spectrum, we conclude that there are no histidine-to-iron charge-transfer transitions evident in the spectra of the proteins.

Recent resonance Raman experiments on oxyhemerythrin suggest the existence of a hydrogen bond between the terminal oxygen of the bound hydroperoxide and the bridging oxygen of the diiron(III) core.[20] It was proposed that such a hydrogen bond could explain the reduced magnetic coupling in oxyhemerythrin ($-J$ = 77 cm^{-1}) compared to that in methemerythrin ($-J$ = 134 cm^{-1}).[21] It is therefore curious that the electronic spectrum of oxyhemerythrin differs little, with the exception of a peroxide-to-metal charge-transfer band at 500 nm, from spectra of the methemerythrins. If such a hydrogen bond were to exist, it must have little effect on the electronic spectrum of the (μ-oxo)diiron(III) core. We were therefore interested to examine the effects of hydrogen-bonding solvents on the spectral and magnetic properties of the model complexes.

(19) Bernarducci, E.; Schwindinger, W. F.; Hughey, J. L. H., IV; Krogh-Jespersen, K.; Schugar, H. J. *J. Am. Chem. Soc.* **1981**, *103*, 1686–1691.
(20) Shiemke, A. K.; Loehr, T. M.; Sanders-Loehr, J. *J. Am. Chem. Soc.* **1984**, *106*, 4951–4956.
(21) Dawson, J. W.; Gray, H. B.; Hoenig, H. E.; Rossman, G. R.; Schredder, J. M.; Wang, R. H. *Biochemistry* **1972**, *11*, 461–465.

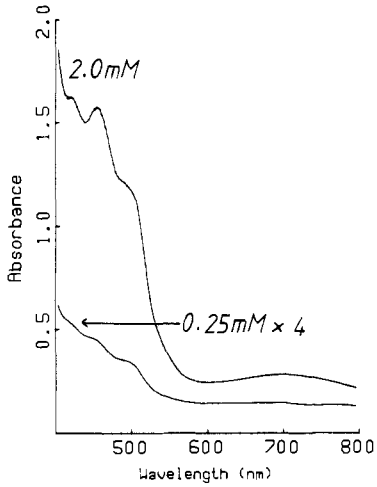

Figure 3. Electronic spectra of **1** in water. Shown are the spectrum of a 0.25 mM solution of **1** (at 4 times the original scale) and the spectrum of a 2.0 mM solution of **1**.

The integrity of **1** after dissolution in acetonitrile, methanol, and water was checked by removing the solvent in vacuo and comparing the infrared spectra of the resulting residues with that of untreated **1**. In all cases they were identical. Thus, dissolving **1** in any of these solvents is unaccompanied by rapid decomposition. Upon standing, however, solutions of **1** in water become cloudy after a few hours and develop a precipitate overnight. This decomposition can be followed by electronic spectroscopy. There is little change within the first hour, however, and the spectrum reported above was recorded in that time period.

Solutions of **1** in water obey Beer's law above 2 mM concentrations. If the concentration is lowered to 0.25 mM, immediate changes occur in the electronic spectrum similar to those taking place over a longer period of time in more concentrated solutions. This effect is illustrated in Figure 3, from which it is apparent that dilute solutions of **1** do not obey Beer's law. The spectrum of **1** in water reported in Table II and discussed below was obtained from solutions exceeding 2.0 mM.

This spectrum is markedly changed from those recorded of acetonitrile and methanol solutions (Figure 2), probably due in large part to hydrogen-bonding interactions. The intensities of all bands in the spectrum are decreased from their values in the organic solvents in the order $CH_3CN > CH_3OH > H_2O$ (Table IV). The d–d band at 743 nm in the methanol spectrum shifts to 701 nm in water, and it has nearly half the intensity. A shoulder at 543 nm in the methanol spectrum has disappeared entirely from the spectrum in water. The possibility that the reduced intensity of the visible spectrum of **1** in H_2O is due to dissociation into monomeric species seems unlikely. The appearance and infrared spectrum of the complex recovered from aqueous solution are substantially unchanged. Moreover, the concentrated aqueous solutions studied here obey Beer's law (vide supra), indicating that no significant monomer/dimer equilibrium exists in these solutions.

The reversible protonation of the oxo bridge in **2** was recently reported by us.[15] The protonated form has an electronic spectrum quite unlike that of **1** or **2** in any solvent. The spectrum of this species is dominated by a single peak at 375 nm and contains d–d bands at 700 and 1115 nm of ordinary intensity for monomeric high-spin iron(III) complexes. It is therefore clear that the spectral changes of **1** in protic solvents are not due to protonation of the oxo bridge, although hydrogen bonding between the bridging oxygen atom and solvent is likely.

Vibrational Spectroscopy. Table V lists the peaks found in the solution resonance Raman spectrum of **1** taken with 514-nm excitation. Although most of these are unassignable, we attribute the band at 274 nm to the Fe–N stretch by analogy to the comparable peak in the spectrum of **2**.[1b] The band at 320 nm may similarly correspond to the Fe–carboxylate oxygen symmetric stretching mode. Isotopic substitutions will be required to confirm these assignments.

Table V. Peaks in the Resonance Raman Spectrum of **1** (between 150 and 950 cm^{-1}) in Acetonitrile at 514-nm Excitation

peak position, cm^{-1}	assignt	peak position, cm^{-1}	assignt
211		608	ligand
274	ν_s, Fe–N	747	solvent
320	ν_s, Fe–O	792	
380	solvent	818	
540	ν_s, Fe–O–Fe	865	
581		917	solvent

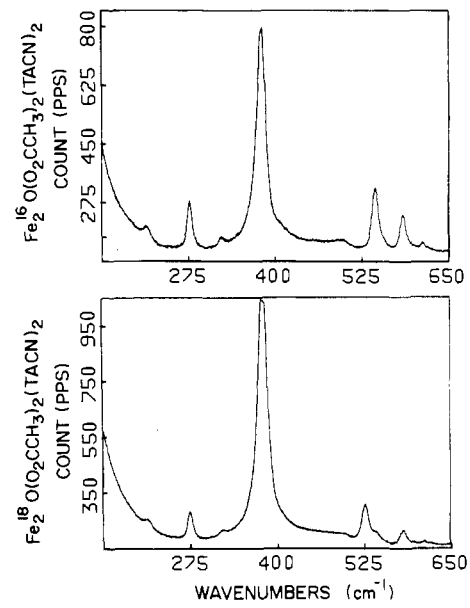

Figure 4. Resonance Raman spectra of **1** (top) and its ^{18}O-substituted derivative (bottom) in CH_3CN solution using 514.5-nm excitation light.

Compound **1** was prepared with ^{18}O in the bridging position in order to identify definitively those bands associated with the oxo bridge. Only one band in the Raman spectrum shifted (Figure 4), from 540 cm^{-1} in the solution spectrum of [^{16}O]**1** to 523 cm^{-1} in the solution spectrum of [^{18}O]**1**. A similar shift occurred in the solid-state spectra where, again, no other band was affected. This shifting band is clearly the symmetrical Fe–O–Fe stretch, similar in energy to that found at 528 cm^{-1} in the spectrum of **2**.[1b] But unlike the spectrum of **2**, the spectrum of **1** contains no peaks assignable to combination bands or deformation modes. These weak bands in the spectrum of **2** may simply not be sufficiently intense to observe in **1**. Careful scrutiny of the spectrum at energies where the asymmetric stretch was expected revealed no shifting band upon isotopic substitution, consistent with the results of the study of compound **2**.[1b]

Both the symmetric and asymmetric Fe–O–Fe vibrations have associated bands in the infrared spectrum of **1**. The FTIR spectra of [^{16}O]**1** and [^{18}O]**1** and the difference spectrum are displayed in Figure 5. The asymmetric stretching band at 749 cm^{-1} shifts to 716 cm^{-1} upon isotopic substitution, while the shift of the symmetric stretching band revealed in the Raman spectra is also observed. The value for the frequency of the asymmetric stretch is similar to that (751 cm^{-1}) observed in the spectrum of **2**.[1b] As observed for **2**, the asymmetric band in the infrared spectrum of **1** is relatively weak compared to those of the simple oxo-bridged diiron(III) complexes, providing further support for the suggestion that the asymmetric stretch is inherently weak for such complexes having small bridging angles.[1b]

Force constants were calculated for the (μ-oxo)diiron(III) core stretching vibrations as described previously,[1b,22] by using all of the data and averaging the values. The stretching force constant k_d was calculated in this manner to be 3.21 mdyn/Å while the stretch–stretch interaction constant k_{dd} was calculated to be 0.21

(22) (a) Wing, R. M.; Callahan, K. P. *Inorg. Chem.* **1969**, *8*, 871–874. (b) Cotton, F. A.; Wing, R. M. *Inorg. Chem.* **1965**, *4*, 867–873.

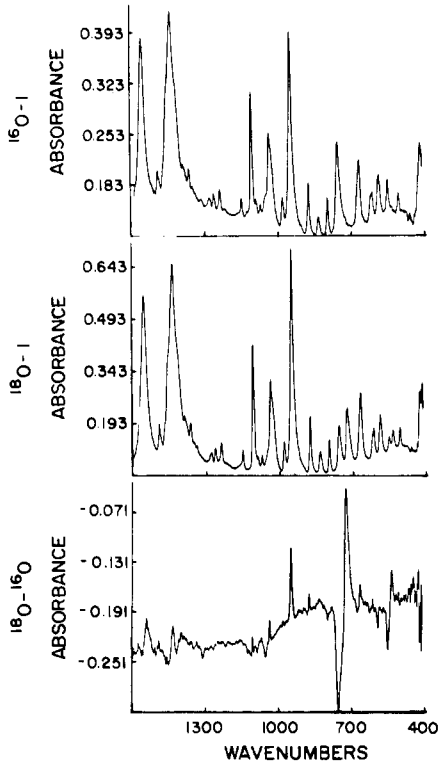

Figure 5. Fourier transform infrared spectra of [^{18}O]**1** and [^{16}O]**1** and the different between these spectra. Samples were run in KBr for 32 scans at 2-cm^{-1} resolution.

Table VI. Comparison of Observed and Calculated Vibrational Frequencies (cm^{-1})

	1				2[a]			
	obsd ^{16}O	calcd ^{16}O	obsd ^{18}O	calcd ^{18}O	obsd ^{16}O	calcd ^{16}O	obsd ^{18}O	calcd ^{18}O
ν_s, M-O-M	540	541	523	522	528	528	511	510
ν_{as}, M-O-M	749	750	716	715	751	751	721	715
force const, mdyn/Å	$k_d = 3.21$, $k_{dd} = 0.21$				$k_d = 3.24$, $k_{dd} = 0.35$			

[a] Reference 1.

mdyn/Å. The stretching force constant is almost identical with that found for **2**, but the interaction constant calculated here is significantly smaller. A comparison of observed and calculated vibrational frequencies for **1** and **2** is given in Table VI. As can be seen, the agreement is excellent.

Excitation Profiles. The excitation profiles, measured from 454 to 577 nm, of selected peaks in the Raman spectrum of **1** are shown in Figure 6. The profile of the weak solvent peak at 747 cm^{-1}, which should be a horizontal straight line, allows one to estimate the errors inherent in these profiles. The other Raman band profiles shown in Figure 6 are for the 540-cm^{-1} band, assigned above as the Fe–O–Fe symmetric stretch (ν_s), the 274-cm^{-1} band, assigned above as the Fe–N stretch, and the 581-cm^{-1} peak, which is unassigned.

The 540-cm^{-1} peak is maximally enhanced upon irradiation at ~520 nm and is also weakly enhanced between 480 and 485 nm. Both of these positions lie between bands in the visible spectrum of **1**. Presumably, weak hidden transitions are responsible for the form of this excitation profile. The profile is very similar to that of the ν_s band of **2**,[23] which is also maximally enhanced at 520 nm, a position that similarly lies between maxima in the electronic spectrum of **2**.[1b] In addition, reinvestigation of the profile of the ν_s band[23] from the Raman spectrum of **2** revealed it also to be weakly enhanced at 480 nm, although the enhancement in this region is even weaker than that observed for the ν_s band of **1** at this wavelength. The nature of the visible electronic transitions responsible for the enhancement of these bands is still not clear.

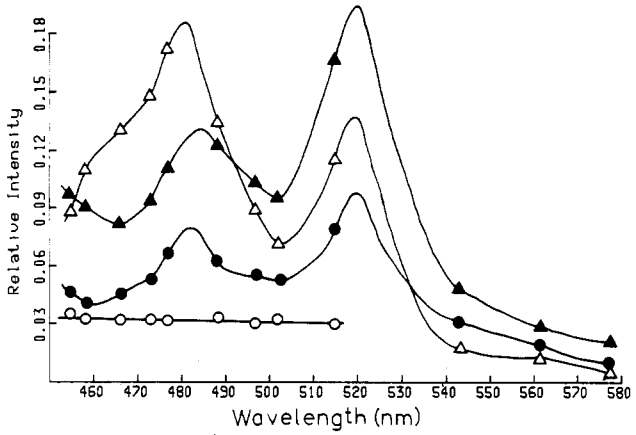

Figure 6. Excitation profiles of (▲) the 540-cm^{-1} (ν_s, Fe–O–Fe), (△) the 274-cm^{-1} (ν_s, Fe–N), (●) the 581-cm^{-1} (unassigned), and (○) the 747-cm^{-1} (solvent) Raman bands from the spectrum of **1** in CH_3CN solution.

The 274-cm^{-1} band is maximally enhanced around 480 nm but also shows enhancement at 520 nm. The enhancement profile of this peak is much more pronounced than that of the comparable band (at 273 cm^{-1}) in the Raman spectrum of **2**, but basically has the same shape.[23] The band in the spectrum of **2** is most intense with excitation in the region 470–475 nm.

It is interesting that the enhancement profile of the unassigned 581-cm^{-1} peak parallels that of the 540-cm^{-1} band. Since this peak does not shift at all upon ^{18}O-isotopic substitution, the 581-cm^{-1} band cannot be assigned as any kind of an Fe–μ-oxo vibration. The fact that its enhancement profile is so similar to that of the ν_s peak suggests that the electronic transitions responsible for the enhancement of these bands are not simply bridging oxygen-to-iron charge-transfer bands but, rather, are transitions that may enhance a variety of different vibrations of the iron center independent of the oxo bridge.

Excitation profiles were also determined for peaks in the Raman spectrum of **1** at 211, 320, and 608 cm^{-1}. The 211-cm^{-1} peak has a profile that parallels that of the 274-cm^{-1} band (Fe–N stretch). The profile of the 320-cm^{-1} peak has its maximum at 475 nm, shifted somewhat from the maxima of the profiles for the other bands discussed above. There is no way of knowing whether this result is consistent with the assignment of this band to the symmetric Fe–carboxylate stretch suggested above. The profile of the 608-cm^{-1} band is essentially a straight line, indicating that this peak is probably due to a ligand vibration.

Conclusions. The electronic spectrum of complexes containing the (μ-oxo)bis(μ-carboxylato)diiron(III) core is conserved despite changes in the nonbridging ligands. The similarity in the electronic structures of $[Fe_2O(O_2CR)_2]^{2+}$ cores containing imidazole (proteins) or pyrazole (models) ligands was expected,[19] but the present study also reveals that even a complex with this core capped by aliphatic triazacyclononane ligands has a similar electronic spectrum. The similarity in the spectra of the different methemerythrin derivatives, with various bound exogenous ligands, provides further support that the electronic spectrum is characteristic of the $[Fe_2O(O_2CR)_2]^{2+}$ core. Resonance Raman and FTIR spectra of **1** show the similarity of its vibrational structure with that of **2** and the hemerythrins.

Solvent effects, especially the presence or absence of hydrogen-bonding interactions, can clearly modulate the electronic structures of these complexes. Oxyhemerythrin, in which it has been suggested that there is a hydrogen bond between the proposed hydroperoxy ligand and the bridging oxygen,[20] has an electronic spectrum quite similar to that of azidomethemerythrin,[13c] although the magnetic coupling between the iron atoms is weaker.[21] It is possible that solvation of **1** by methanol or water provides a good model for this suggested hydrogen-bonding interaction in oxyhemerythrin.

(23) Spool, A. Ph.D. Dissertation, Columbia University, 1985.

Acknowledgment. This work was supported by National Institutes of Health Research Grant GM 32134 from the National Institute of General Medical Sciences. Raman spectra were obtained at the MIT Regional Laser Center, which is a National Science Foundation Regional Instrumentation Facility.

Registry No. 1, 96502-25-9; 2, 86177-70-0.

Supplementary Material Available: Tables S1 and S2, reporting observed and calculated structure factor amplitudes and thermal parameters for non-hydrogen atoms (8 pages). Ordering information is given on any current masthead page.

Contribution from Chemistry Department A, The Technical University of Denmark, DK-2800 Lyngby, Denmark

Chloro Complexes in Molten Salts. 10. Potentiometric and Spectrophotometric Study of the System $KCl-AlCl_3-CuCl_2$ at 300 °C

J. H. VON BARNER,* P. B. BREKKE, and N. J. BJERRUM*

Received December 12, 1983

The formation of complexes of Cu(II) in $KCl-AlCl_3$ melts at 300 °C (in some cases saturated with $CuCl_2$) has been studied by potentiometric and spectrophotometric measurements. With the Cu(II) concentration in the range 0.10–1 M and with the pCl range 0.38–6.0 the results could be explained by the following equilibria: (i) $CuCl_4^{2-} \rightleftarrows CuCl_3^- + Cl^-$; (ii) $CuCl_3^- \rightleftarrows CuCl_2 + Cl^-$; (iii) $CuCl_2 \rightleftarrows CuCl^+ + Cl^-$; (iv) $CuCl_2(soln) \rightleftarrows CuCl_2(s)$. p$K$ values (based on molar concentrations) for reactions i–iii: for 0.10 M Cu(II), 1.14 (4), 3.17 (26), 5.4 (3); for 0.31 M Cu(II), 0.99 (2), 3.29 (2), no value found; for 1 M Cu(II), 0.79 (4), 3.55 (3), no value found. By comparison, the pK for reaction i calculated from spectrophotometric measurements on 0.10 M solutions of Cu(II) in $KCl-AlCl_3$ melts at 300 °C was in the range −0.1 to +1.9. The maximum obtainable molar concentration of $CuCl_2$ (determined by reaction iv) was from the potentiometric measurements calculated to be 0.005 (3). This is in good agreement with a value of 0.0031 (8) obtained from the spectrophotometric measurements. Finally, the spectra of $CuCl_4^{2-}$, $CuCl_3^-$, and $CuCl_2$ were calculated from measured spectra of $KCl-AlCl_3-CuCl_2$ melts.

Introduction

The Cu(II) complexes formed in the $KCl-AlCl_3-CuCl_2$ system were examined as part of a general examination of solute species in chloroaluminate melts. However, it is also interesting to note that related systems such as $KCl-CuCl_2/CuCl-LaCl_3$ and $KCl-CuCl/CuCl_2$[1-3] melts have industrial applications due to their catalytic properties.

Not much work has been performed concerning the identity of the formed Cu(II) species in the related alkali chloride melts,[4-7] and almost nothing seems to be known of the species in alkali chloride–aluminum chloride melts; however, an examination of $CuCl_2$ in liquid aluminum chloride has been reported.[8]

In melts with very high chloride activity such as molten CsCl,[6] the presence of the tetrahedral coordinate copper(II) was based on comparison with solid Cs_2CuCl_4 and Cs_2ZnCl_4 (doped with Cu^{2+}), which both have known crystal structures. Also in the LiCl–KCl eutectic melt the observed spectra of Cu(II) were believed to be due to tetrahedral coordinate copper(II), though somewhat distorted.[5]

Due to the rather few experiments made on chloride melts, it is useful to compare these results with experiments made in other nonaqueous solvents such as acetonitrile,[9,10] anhydrous acetic acid,[11] dimethylformamide,[12] propylene carbonate,[13] and dimethyl sulfoxide.[13] The main results of these measurements seem to indicate formation in the dilute systems of the mononuclear complexes $CuCl^+$, $CuCl_2$, $CuCl_3^-$, and $CuCl_4^{2-}$. The complexes are in some cases strongly solvated in some cases probably very weakly solvated.

In connection with an examination of acidic chloroaluminate melts, it is also interesting to make comparison with recent results on complex formation in the gaseous phase between $CuCl_2$ and aluminum chloride. Raman and visible–ultraviolet spectra have shown that copper(II) chloride forms gas-phase complexes such as $CuAl_2Cl_8$ and $CuAlCl_5$.[14-16] The most likely structure of the first compound is a distorted-octahedral structure (with $AlCl_4^-$ as a tridentate ligand) or a square-planar structure (with $AlCl_4^-$ as a bidentate ligand[17]). The structure of the second compound can be visualized as a tetracoordinated copper atom with one chloride and one tridentate $AlCl_4^-$ ligand.

Experimental Section

The chemicals used for the solvent were prepared in the same way as in recent work dealing with $KCl-AlCl_3$ melts.[18] The $CuCl_2$ used was obtained by a method described and evaluated previously.[19]

In some of the experiments where it was necessary to add very small amounts of copper to the melt, a special procedure was applied. The phase diagram for aluminum–copper[20] shows that with a copper content smaller than 5.65 wt % completely miscibility in the solid phase is obtained at 548 °C. The solubility of copper in aluminum decreases rapidly as the temperature decreases; however, in alloys with less than 4–5 wt % copper it is easy to keep the copper homogeneously dissolved in the aluminum by rapid cooling to room temperature. An alloy containing 98.49 wt % aluminum (99.999% pure) and 1.51 wt % Cu (99.99% pure)

(1) Ruthven, D. M.; Kenney, C. N. *Chem. Eng. Sci.* **1967**, *22*, 1561.
(2) Ruthven, D. M.; Kenney, C. N. *Chem. Eng. Sci.* **1968**, *23*, 981.
(3) (a) Riegel, H.; Schindler, H. D.; Sze, M. C. *Chem. Eng. Prog.* **1973**, *69*, 89. (b) *AIChE Symp. Ser.* **1973**, *69* (No. 135), 96.
(4) Harrington, G.; Sundheim, B. R. *Ann. N.Y. Acad. Sci.* **1960**, *79*, 950.
(5) Gruen, D. M.; McBeth, R. L. *Pure Appl. Chem.* **1963**, *6*, 23.
(6) Smith, G. P.; Griffith, T. R. *J. Am. Chem. Soc.* **1963**, *85*, 4051.
(7) Wilmshurst, J. K. *J. Chem. Phys.* **1963**, *39*, 1779.
(8) Øye, H. A.; Gruen, D. M. *Inorg. Chem.* **1964**, *3*, 836.
(9) Manahan, S. E.; Iwamoto, R. T. *Inorg. Chem.* **1965**, *4*, 1409.
(10) Baaz, M.; Gutmann, V.; Hampel, G.; Masaguer, J. R. *Monatsh. Chem.* **1962**, *93*, 1416.
(11) Sawada, K.; Ohtaki, H.; Tanaka, M. *J. Inorg. Nucl. Chem.* **1972**, *34*, 3455.
(12) Elleb, M.; Meullemeestre, J.; Schwing-Weil, M. J.; Vierling, F. *Inorg. Chem.* **1980**, *19*, 2699.
(13) Elleb, M.; Meullemeestre, J.; Schwing-Weil, M. .; Vierling, F. *Inorg. Chem.* **1982**, *21*, 1477.
(14) Emmenegger, F. P.; Rohrbasser, C.; Schläpfer, C. W. *Inorg. Nucl. Chem. Lett.* **1976**, *12*, 127.
(15) Schläpfer, C. W.; Rohrbasser, C. *Inorg. Chem.* **1978**, *17*, 1623.
(16) Papatheodorou, G. N.; Capote, M. A. *J. Chem. Phys.* **1978**, *69*, 2067.
(17) Brooker, M. H.; Papatheodorou, G. N. In "Advances in Molten Salt Chemistry"; Mamantov, G., Ed.; Elsevier: Amsterdam, Oxford, New York, Tokyo, 1983; Vol. 5.
(18) von Barner, J. H.; Bjerrum, N. J.; Smith, G. P. *Acta Chem. Scand., Ser. A* **1978**, *A32*, 837.
(19) Andreasen, H. A.; Mahan, A.; Bjerrum, N. J. *J. Chem. Eng. Data* **1981**, *26*, 195.
(20) Kirk-Othmer "Encyclopedia of Chemical Technology", 2nd ed.; Wiley Interscience: New York, London, 1963; Vol. 1, p 958.

0020-1669/85/1324-2162$01.50/0